HHS Public Access

Author manuscript

Inorg Chem. Author manuscript; available in PMC 2017 November 03.

Published in final edited form as:

Inorg Chem. 2017 August 07; 56(15): 9044–9054. doi:10.1021/acs.inorgchem.7b01022.

Intramolecular C–H and C–F Bond Oxygenation by Site-Differentiated Tetranuclear Manganese Models of the OEC

Kurtis M. Carsch, **Graham de Ruiter**, and **Theodor Agapie***

Division of Chemistry and Chemical Engineering, California Institute of Technology, 1200 East California Boulevard, MC 127-72, Pasadena, California 91125, United States

Abstract

The dangler manganese center in the oxygen-evolving complex (OEC) of photosystem II plays an important role in the oxidation of water to dioxygen. Inspired by the structure of the OEC, we synthesized a series of site-differentiated tetra-manganese clusters $[LMn_3(PhPz)_3OMn]$ $[OTf]x$ (**2**: x = 2; **3**: x = 1) that features an apical manganese ion – distinct from the others – which is appended through an μ_4-oxygen atom bridge to a trinuclear manganese core. This cluster design was targeted to facilitate studies of high-valent Mn-oxo formation, which is a proposed step in the mechanism for water oxidation by the OEC. Terminal Mn-oxo species – supported by multinuclear motif – were targeted by treating 2 and 3 with iodosobenzene. Akin to our previously reported iron complexes, intramolecular arene hydroxylation was observed to yield the C–H bond oxygenated complexes $[LMn_3(PhPz)_2(OArPz)OMn][OTf]_x$ (**5** : x = 2; **6**: x = 1). The fluorinated series $[LMn_3(F2ArPz)_3OMn]$ $[OTf]_x$ (**8** : x = 2; **9**: x = 1) was also synthesized in order to mitigate the observed intramolecular hydroxylation. Interestingly, treating 8 and 9 with iodosobenzene results in intramolecular arene C–F bond oxygenation as judged by electrospray ionization mass spectrometry (ESI-MS). The observed aromatic C–H and C–F hydroxylation is suggestive of a putative high-valent terminal metal-oxo species and it is one of the very few examples capable of oxygenating C–F bonds.

TOC Synopsis

This study describes novel manganese clusters that model structural aspects of the OEC. Upon treatment with an O-atom transfer reagent, iodosobenzene, these complexes oxygenate aromatic C–H and C–F bonds, as evidenced by ^{1}H NMR spectroscopy, mass spectrometry, and independent synthesis of the resulting oxygenated products. The observed reactivity suggests the formation of a high-valent Mn-oxo species.

***Corresponding Author**: agapie@caltech.edu.

ASSOCIATED CONTENT

For additional synthetic procedure, Figures S1–S34, Tables S1 and S2, and crystallographic information files. The Supporting Information is available free of charge on the ACS Publications website at DOI:

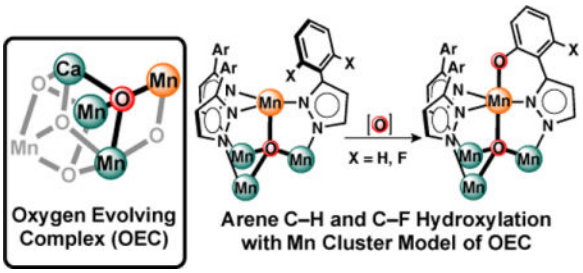

Introduction

Biological water oxidation to O_2 occurs at the oxygen evolving complex (OEC) in photosystem II (PSII).[1] The active site consists of a multinuclear cluster of manganese and calcium ions that are bridged by oxide moieties displaying a cubane motif [Mn_3CaO_4].[2] Appended to this cubane, via a μ_4-oxo bridge, is a fourth manganese center ("dangler"), proposed to coordinate at least one substrate water molecule.[2] Multiple oxidations and deprotonations convert this water molecule to either a terminal or bridging oxo moiety, which ultimately forms the O–O bond.[3] Despite our current understanding, several aspects of water oxidation by the OEC remain unknown.[1b] Nonetheless, understanding the structure-function relationships within the OEC is important, as this knowledge can contribute towards developing new technologies relying on water oxidation.[4]

Towards this end, structurally related synthetic model complexes can provide valuable information by allowing structure-functions, without the added complexity of the native enzyme.[5] For instance, the [Mn_3CaO_4] cubane motif in the OEC has been successfully reproduced in a few synthetic model complexes,[6] some of them even incorporating an additional fifth "dangling" metal ion.[6a–c] However, none of these complexes have been reported to support terminal high-valent Mn-oxo motifs.

The formation of such a terminal Mn-oxo species is an important step in some of the proposed mechanisms for water oxidation by the OEC.[1b] Several synthetic complexes featuring high-valent Mn(IV) or Mn(V)-oxo species have been reported, and are supported with ligands that include porphyrins,[7] corroles,[8] corrolazines,[9] or other types of macrocyclic ligands.[10] Furthermore, a series of Mn(III)-,[11] Mn(IV)-,[12] and Mn(V)- oxo[13] complexes supported by tetradentate tripodal ligands have been reported, where the Mn(V)-oxo models the manganese dangler in its highest oxidation state.[13–14] The electronic description of this Mn(V)-oxo is of particular importance, and highly relevant for mechanistic proposals involving O–O bond formation.[14–15] Other Mn-oxo complexes with similar coordination environments have also been reported.[16] Despite the prevalence of high-valent terminal metal-oxo motifs on monometallic complexes, such motifs on multimetallic scaffolds are scarce and have only been observed or proposed in bimetallic complexes,[17] discrete tetra or penta-nuclear clusters,[18] or polyoxometallates.[19] Notwithstanding, the synthesis and characterization of well-defined multimetallic clusters containing terminal Mn-oxo moieties will provide valuable information regarding its electronic structure and reactivity, data highly relevant for the OEC in PSII.

Recently, we reported the synthesis of a series of well-defined tetranuclear clusters containing a triiron core and a fourth apical Fe or Mn metal center.[18b, 20a] These clusters are capable of intramolecular C(sp^2)−H and C(sp^2)−F bond oxygenation, most likely facilitated by a putative high-valent terminal metal oxo moiety.[18b, 20a]

Modeling the structural features of the OEC including the dangler (Figure 1), we describe herein a series of tetranuclear manganese clusters and their reactivity with oxygen atom transfer (OAT) reagents. Related Mn_4 clusters displaying hydrogen bonding interactions have been shown very recently to support electrochemical water oxidation to H_2O_2.[20b] The clusters $[LMn_3(PhPz)_3OMn][OTf]_x$ (**2**: x = 2; **3**: x = 1) contain three six-coordinate manganese ions related by pseudo-C_3 axis and a fourth (site-differentiated) lower coordinate manganese center, which is appended to the other three metal centers through a μ_4-oxygen atom and three phenyl pyrazolate ligands (Figure 1). Treating these clusters with OAT reagents resulted in intramolecular C(sp^2)−H oxygenation of the bridging phenyl pyrazole ligand. This type of reactivity is consistent with the formation of a reactive Mn-oxo. Although this reactivity has been observed for analogous multimetallic iron complexes,[18b] the oxygenation of C(sp^2)−H bonds by multimetallic manganese complexes is rare.[21] To mitigate intramolecular oxidation, the analogous clusters $[LMn_3(F_2ArPz)_3OMn][OTf]_x$ (**7**: x = 2; **8**: x = 1) were synthesized. The structure and reactivity of these complexes with OATs are discussed as well.

Results and discussion

The envisioned complexes $[LMn_3(PhPz)_3OMn][OTf]_x$ (**2**: x = 2, **3**: x = 1) were synthesized according to a previously reported procedure for $[LFe_3(PhPz)_3OFe][OTf]_x$ (x = 1–3).[22] Starting from $LMm(OAc)(OTf)_2$, addition of sodium 3-phenyl-pyrazolate (NaPhPz; 3.2 equiv.) followed by oxidation with iodosobenzene (PhIO; 1.1 equiv.) yielded a purple-brown powder with ^{1}H-NMR spectrum distinct from $LMn_3(OAc)(OTf)_2$ (Figure S1 and S2). This intermediate was tentatively assigned as $[LMn_3(PhPz)_3ONa][OTf]$ (1) based on its ESI-MS spectrum (Figure S18; m/z = 1488.3). Complex 1 was crystallized before salt metathesis with $Mn(OTf)_2$·2MeCN (2.0 equiv.) to yield the tetra-nuclear manganese complex $[LMn_3(PhPz)_3OMn]$ $[OTf]_2$ (2) in *ca.* 45% yield (Scheme 1).

Single crystals suitable for X-ray diffraction (XRD) were obtained by vapor diffusion of diethyl ether into a concentrated solution of 2 in acetonitrile. Complex 2 displays a $[Mn_4$-O)] cluster, with three manganese ions supported by bridging alkoxides and nitrogen donors from ligand L, while the distinct fourth Mn is bridged by pyrazolates (Figure 2A). The metals bound to ligand L, described as the basal trinuclear core, are all six-coordinate. The apical metal, modeling the dangler Mn, is five-coordinate with three pyrazolate ligands, a μ_4-O donor, and one acetonitrile in the coordination sphere. Two outer sphere triflate counter ions are present. Based on charge balance, complex 2 displays two Mn(III) and two Mn(II) metal centers. The three basal pseudo-octahedral manganese centers (Mn1–Mn3) are connected via a μ_4-oxo bridge. Based on the Mn1–O1 (2.240(3) Å), Mn2–O1 (1.886(3) Å), and Mn3–O1 (1.891(3) Å) bond distances, the oxidation state of the trimanganese core is assigned as $Mn^{III}_2Mn^{II}$. The observed bond metrics in 2, are comparable to other complexes featuring similar $[Mn_4(\mu_4$-O)] core geometries,[23] supporting the discrete oxidation state

assignments of the individual manganese metal centers. The relatively long Mn1–N13 bond distance of 2.159(4) Å – compared to the Mn2–N23 (2.011(3) Å) and Mn3–N33 (1.998(3) Å) bond distances – corroborates this assignment (Table 1). The apical manganese metal center (Mn4) is trigonal bipyramidal ($\tau_5 = 0.79$)[24] and connected to the trimanganese core through a μ_4-oxo bridge (O1). The apical manganese ion is assigned as Mn(II) based on charge balance and the long Mn4–O1 bond distance of 2.108(3) τ.[23d23e] The overall oxidation state of 2 is thus assigned as $[LMn^{II}Mn^{III}_2(PhPz)_3OMn^{II}][OTf]_2$, analogous to our previously reported iron complexes.[18b22]

The cyclic voltammogram (CV) of 2 shows two distinct quasireversible redox events at −1.67 V ($[Mn^{II}_4]^0/[Mn^{II}_3Mn^{III}]^{1+}$) and at −0.60 V ($[Mn^{II}_3Mn^{III}]^{1+}/[Mn^{II}_2Mn^{III}_2]^{2+}$) vs. Fc/Fc^+ (Figure 3). An additional irreversible redox event, corresponding to the $[Mn^{II}_2Mn^{III}_2]^{2+}/[Mn^{II}Mn^{III}3]^{3+}$ redox-couple, was found at more positive potentials *(ca.* 0.21 V). The deviation from reversible electrochemical behavior is attributed to large structural rearrangements upon oxidizing Mn(II) to Mn(III). In particular, the population of the d_{z2} σ-antibonding orbital results in bond elongation along the z-axis. Irreversible or quasireversible behavior has been observed for other multimetallic manganese complexes.[5f, 25] Such structural distortions are absent in the analogous iron-manganese complex $[LFe_3(PhPz)_3OMn][OTf]_2$, where three reversible one electron oxidation processes are observed.[18b] Indeed, for compound 2, large distortions are observed in the Mn-O(alkoxide) distances (*Δ*Mn–O = 0.34 Å), while for corresponding iron complexes, these distortions are significantly lower (*Δ*Fe–O = 0.15 Å).[18b, 22]

The electrochemical studies indicate that the reduced or oxidized complexes $[LMn_3(PhPz)_3OMn][OTf]_x$ (x = 1 or 3) might be accessed through chemical oxidation/reduction. While the addition of silver triflate (AgOTf; 1.1 equiv.) resulted in the formation of an intractable mixture, addition of cobaltocene ($CoCp_2$; 1.1 equiv.) to a solution of **2** in CH_2Cl_2, resulted in a markedly different ^{1}H NMR spectrum, attributed to a new paramagnetic species 3 (Figure S4).

This new paramagnetic species was assigned as $[LMn_3(PhPz)_3OMn][OTf]_1$ based on single crystal XRD (Figure 2B). The coordination environment around the apical manganese metal center (Mn4) is trigonal pyramidal. The distance between the centroid defined by the Mn1|Mn2|Mn3 trigonal plane (Mn_{core}) and O1, elongates from 0.913 Å to 0.962 Å upon reduction from **2** to **3**. The elongation is proposed to result from decrease in Lewis acidity of the Mn_{core}, weakening the interaction with O1. Other notable differences are observed in the Mn_{core}–O1 distances. Consistent with the reduction of a Mn(III) metal center, the Mn2–O1 bond distance elongates from 1.886(3) Å in **2** to 2.189(2) Å in **3**, supporting an overall $Mn^{III}Mn^{II}_2$ oxidation state assignment of the trimanganese core.[23]

With isostructural complexes **2** and **3** in hand, we investigated their abilities to access high-valent terminal metal-oxo species. The differences in oxidation state of the trimanganese core ($\mathbf{Mn^{III}_2Mn^{II}}$ vs. $\mathbf{Mn^{III}Mn^{II}_2}$) could influence the electronic structure or reactivity of the terminal metal-oxo moiety (i.e. nucleophilic vs. electrophilic).[26] Addition of iodosobenzene (PhIO; 1.1 equiv.) to complexes **2** and **3** afforded brown-black species with a highly complicated ^{1}H-NMR spectrum (Figures S7 and S11). The ^{1}H NMR spectra are

difficult to interpret due to paramagnetic broadening by manganese. This is contrast to the ^{1}H NMR spectra previously reported for iron complexes, for which sharper NMR resonances could be observed.[22] However, ESI-MS analysis of the reaction mixtures showed single peaks corresponding to $[LMn_3(PhPz)_2(OArPz)OMn]^{2+}$ (**5**; *m/z* = 767.8) and $[LMn_3(PhPz)_2(OArPz)OMn]^{1+}$ (**6**; *m/z*= 1534.8), consistent with an overall process corresponding to intramolecular C(sp^2)–bond oxygenation of the surrounding ligand scaffold (Figure S21 and S23). Unfortunately, repeated crystallization from the reaction mixture did not result in X-ray quality crystals of the tentatively assigned complexes $[LMn_3(PhPz)_2(OArPz)OMn][OTf]_2$ (**5**) and $[LMn_3(PhPz)_2(OArPz)OMn][OTf]_1$ (**6**).

To verify arene hydroxylation, complexes **5** and **6** were synthesized independently (Figure 4). Addition of sodium 2 (pyrazol-3-yl)phenolate (NaOArPzH; 1.1 equiv.) to complex **2** resulted in the formation of **6** (Figure S9). One electron oxidation with AgOTf (1.0 equiv.) resulted in the formation of **5** (Figure S6). Both independently synthesized complexes show nearly identical ESI-MS and ^{1}H NMR spectra when compared to the crude reaction mixtures of **2** and **3** respectively, confirming that intramolecular C–H bond oxygenation is the most probable reaction pathway (Figure S8, S12, S22, and S24)

Previous studies have indicated that intramolecular C(sp^2)– H bond oxygenation is preceded by rate-limiting oxygen atom transfer from an iodosobenzene-adduct, most likely generating a high-valent terminal Mn^{IV}-oxo.[18b] Given the similar reactivity of 1 and previously reported $[LFe_3(PhPz)_3OMn][OTf]_2$, a high-valent terminal Mn-oxo might be involved in the intramolecular C(sp^2)-H bond oxygenation. This is notableas an example of a Mn4 cluster structurally reminiscent of the OEC that supports reactive terminal Mn-oxo CH oxygenation.

Definite structural evidence for C–H bond oxygenation was provided by X-ray crystallography (Figure 2C). Single crystals of the phenoxide-coordinated cluster ($[LMn_3(PhPz)_2(OArPz)OMn][OTf]_1$, **6**) could be obtained only after substituting of the outer sphere anion with tetraphenylborate (**6′**; see the supporting information for experimental details). Complex **6′** shows the oxygenated phenylpyrazole ligand, where O2 is coordinated to the apical manganese center (Mn4). The Mn_{core}–O1 bond distances of 2.179(3) Å (Mn1–O1), 2.274(3) Å (Mn2–O1), and 1.904(3) Å (Mn3– O1), resemble those of 3 (Table 1) and indicate no changes in the Mn_{core} oxidation states ($Mn^{II}_2Mn^{III}$). The contraction of Mn4–O1 bond distance from 2.108(3) Å to 1.851(3) Å) suggests oxidation of the apical manganese metal center from Mn^{II} to Mn^{III}.[23] Similar to related iron-based systems, oxidation exclusively occurs at the site-differentiated metal center.[18b, 20a] These results indicate that formed oxidizing species – postulated to be a high-valent Mn(IV)=O motif – are competent for hydroxylation of strong C–H bonds. High valent Mn-oxo motifs have similarly been invoked as key intermediates in olefin epoxidation,[27] C–H bond hydroxylation,[28] hydride transfer,[29] and hydrogen peroxide disproportionation.[30]

In order to avoid the observed intramolecular oxygenation, 3-(2,6-difluorophenyl)pyrazole was selected as bridging ligand to eliminate C–H bonds that are sterically accessible to the proposed metal-oxo moiety. Furthermore, the oxygenation of C–F bonds by metal oxo species is very rare.[20, 31] Consequently ligand fluorination might prevent the oxygenation reaction, allowing potential characterization of a transient terminal Mn(IV)-oxo

intermediate. Complexes of the general formula $[LMn_3(F_2ArPz)OMn][OTf]_x$ (**8**: x = 2; **9**: x = 1; F_2ArPz = 3 (2,6-difluorophenyl)pyrazolate) were synthesized according to the procedure outlined in Scheme 1. Complexes **8** and **9** were characterized by single crystal X-ray diffraction. The solid-state structure of **9** (Figure 5) is quite different than that of **2**. An interaction between the manganese metal center (Mn4) and one of the *ortho* fluorine substituent (F4) is observed. The Mn4–F4 distance of 2.469(1) is significantly shorter than the sum of the corresponding van der Waals radii (3.55 Å).[32] Additionally, this interaction is evident from the inward orientation of one of phenyl rings of the pyrazolate ligands (Figure 5). Such an interaction is absent in **8**, where acetonitrile is coordinated to the apical metal center (Figure S33). The bond metrics are similar to those of 3. For example, the Mn1–O1 (2.127(1) Å), Mn2–O1 (2.192(2) Å) and Mn3–O1 (1.801(1) Å) suggest an overall $[Mn^{II}_2Mn^{III}]$ oxidation state for the trimanganese core, as in **3**. Compared to **8**, the Mn2–O1 bond distance has elongated from 1.914(3) (**8**) to 2.192(2) (**9**) indicative of reduction from Mn^{III} to Mn^{II} (Table 1). Based on charge balance, the manganese oxidation states **9** are assigned as $[LMn^{II}_2Mn^{III}(F_2ArPz)_3OMn^{II}][OTf]_2$.

Continuing our efforts to target a high-valent terminal Mn(IV)-oxo, complexes **8** and **9** were treated with PhIO (1.1 equiv.). The ESI-MS spectrum – taken from the crude reaction mixtures – showed peaks corresponding to $[LMn_3(F_2ArPz)_2(OFArPz)OMn]^{2+}$ (10; m/z = 812.7) and $[LMn_3(F_2ArPz)_3OMnF]^{2+}$ (11; m/z = 823.7) for the reaction of PhIO with complex **8**, or peaks corresponding to $[LMn_3(F_2ArPz)_2(OFArPz)OMn]^{+}$ (12; m/z = 1624.9) and $[LMn_3(F_2ArPz)_3OMnF]^{2+}$ (**13**; m/z = 1646.8) for the reaction of PhIO with complex **9** (Figures S28 and S29). As described for the Fe analogs, these reactions correspond to C–F bond oxygenation coupled to fluoride and electron transfer to starting cluster **8** (or **9**). Unfortunately, the tentatively assigned complexes **10–13** could not be isolated in analytically clean form by repeated crystallization of the reaction mixtures. Independent synthesis was also problematic for a variety of reasons, including selectivity of metallations and solubility differences. Sufficient characterization data for complexes **10–13** was not obtained to undoubtedly assign them as the $C(sp^2)$-F bond oxygenation products. Moreover, the highly complicated ^1H NMR spectrum of the crude reaction mixture – containing at least two different species given the nature of the reaction – precluded us from making meaningful comparison based on ^1H NMR alone (Figures S16 and S17). Notwithstanding, the ESI-MS data does reveal that complexes **8** and **9** are capable of intramolecular $C(sp^2)$–F bond oxygenation, which has rarely been observed with Mn,[33] and is exceedingly rare with other metal complexes.[20, 31a–f]

For general C–H bond oxygenation, three general mechanisms are envisioned: (i) direct C–H activation by an iodosobenzene adduct, (ii) H-atom abstraction from the proximal C– H with subsequent radical rebound, or (iii) electrophilic activation via the **π** system of the arene (Figure 6). Mechanism (i) proceeds through concerted C–H insertion and elimination of iodobenzene, avoiding the formation of a high-valent terminal Mn-oxo. Direct substrate oxygenation from manganese-oxidant adducts has been reported.[7a, 34] Mechanisms (ii) and (iii) invoke the formation of a transient high-valent terminal Mn-oxo species. Computational studies have suggested that mechanism (iii) is the preferred reaction pathway for arene hydroxylation in cytochrome P450.[35] Such a mechanism might also be operating in the

present study. Recently, we observed and crystallographically characterized an unusual iodosobenzene adduct on a heterobimetallic cluster featuring a similar site-differentiated manganese metal center.[18b] These studies suggested that a Mn-oxo species, rather than an intermediate iodosobenzene adduct, is most likely responsible for the observed arene activation. In line with the proposed mechanism for benzene hydroxylation by P450,[35] a putative Mn(IV)-oxo species generated at the apical metal and is expected to perform initial electrophilic attack on the π-system of the arene ring at the closest accessible position. In the present system, the corresponding phenoxide is generated, with the overall loss of an H-atom.[18b,20,36]

Related mechanisms have been proposed for haloarene hydroxylation with iron-oxo species.[31b,37] Computational studies of a mononuclear iron complex competent for C–F bond oxygenation support a mechanism involving electrophilic arene attack by an observable high-valent Fe(IV)-oxo species.[31b] Similarly, for the clusters reported here, an intermediate terminal Mn(IV)-oxo species could undergo electrophilic attack on the arene π-system, followed by rearomatization by expelling a fluorine anion. Additionally, for multinuclear systems, intramolecular electron transfer between manganese metal centers is possible. One-electron reduction of a high-valent Mn(IV)-oxo by a basal Mn(II) center to form a basal Mn(III) site and a Mn(III)-oxide that undergoes nucleophilic aromatic substitution cannot be ruled out based on the current results. Overall, such nucleophilic aromatic substitution results in the same overall transformation as by an electrophilic mechanism. Noting that the crystal structure of **9** shows an interaction between the arene F substituent and the manganese center (Figure 5), C–F bond cleavage may be facilitated by metal coordination to the fluorine moiety. However, displacement of the aryl-fluoride ligand by acetonitrile in **8** suggests that upon coordination of an additional ligand, such as the oxygen atom transfer reagent, fluoride binding is disfavored.

Summary

Inspired by the site-differentiation of the oxygen-evolving complex of photosystem II (Scheme 1), two series of tetra-manganese clusters with general formulae $[LMn_3(PhPz)_3OMn][OTf]_x$ (**2**: x = 2; **3**: x = 1) and $[LMn_3(F_2ArPz)_3OMn]$ $[OTf]_x$ (**8**: x = 2; **9**: x = 1) were synthesized. Addition of iodosobenzene (PhIO) to **2** and **3** resulted in C–H bond oxygenation of the bridging phenyl pyrazolate, while addition of PhIO to **8** and **9** resulted in highly unusual arene C– F bond oxygenation. These studies suggest that the formation of putative high-valent terminal Mn-oxo motifs on multimetallic scaffolds is possible. These reactive species are of interest in the context of modeling the function of the OEC. Current efforts are focused on addressing the effect of cluster structure and composition on reactivity.

EXPERIMENTAL SECTION

General Considerations

All reactions were performed at room temperature in an N_2-filled M. Braun Glovebox or by using standard Schlenk techniques unless otherwise specified. Glassware was oven dried at 140 °C for at least 2 h prior to use, and allowed to cool under vacuum. All reagents were

used as received unless otherwise stated. Sodium 5-phenylpyrazolate (NaPhPz),[20a] sodium 5-(2,6-difluoro)phenylpyrazolate (NaF2ArPz),[20a] sodium 2-(1*H*-pyrazol-5-yl)phenolate (NaOArPzH),[20a] sodium 3-fluoro-2-(1*H*-pyrazol-5 yl)phenolate (NaOFArPzH),[20a] iodosobenzene (PhIO),[38] silver tetraphenylborate ($AgBPh_4$),[39] and $Mn(OTf)_2(MeCN)_2$[40] were prepared according to literature procedures. Caution! *PhIO is a potential explosive and should therefore be synthesized and stored in minimal quantities*. MeOTf, $Na(N(SiMe_3))$, and AgOTf were purchased from Sigma Aldrich and Strem Chemicals. Cobaltocene (Cp_2Co) and decamethylcobaltocene (Cp^*_2Co) were purchased from Strem Chemicals and sublimed before use. Anhydrous tetrahydrofuran (THF) was purchased from Aldrich in 18 L Pure-Pac™ containers. Anhydrous CH_2Cl_2, diethyl ether, hexane and THF were purified by sparging with nitrogen for 15 minutes and then passing under nitrogen pressure through a column of activated A2 alumina. Anhydrous 1,2-dimethoxyethane (DME) was dried over sodium/benzophenone and vacuum-transferred onto molecular sieves. The ^1H and ^{19}F NMR spectra were recorded at 300.13 and 282.36 MHz, respectively, on a Varian 300 MHz spectrometer. All chemical shifts (δ) are reported in ppm, and coupling constants *(J)* are in Hz. The ^1H NMR spectra were referenced using residual solvent peaks in the deuterated solvent. The ^{19}F chemical shifts are reported relative to the internal lock signal. Deuterated solvents (CD_2Cl_2 and CD_3CN) were purchased from Cambridge Isotope Laboratories, dried over calcium hydride, degassed by three freeze-pump-thaw cycles and vacuum transferred prior to use. The UV-vis spectra were recorded on a Varian Cary Bio 50 spectrophotometer. Fast atom bombardment-mass spectrometry (FAB-MS) analysis was performed with a JEOL JMS-600H high-resolution mass spectrometer. Elemental analyses were performed at Caltech.

Electrochemical measurements

CVs were recorded with a Pine Instrument Company AFCBP1 bipotentiostat using the AfterMath software package. All measurements were performed in a three-electrode cell configuration that consisted of (1) a glassy-carbon (ϕ = 3.0 mm) working electrode, (2) a Pt wire as the counter electrode, and (3) an Ag wire as the reference electrode. All electrochemical measurements were performed at RT in an M. Braun N_2-filled glovebox. Dry dichloromethane or acetonitrile that contained 0.1 M Bu_4NPF_6 was used as the electrolyte solution. The ferrocene/ferrocenium (Fc/Fc^+) redox couple was used as an internal standard for all measurements.

X-ray crystallography

For compounds **2**, **3**, **6′**, and **9**, low temperature (100 K) diffraction data (ϕ-and ω-scans) were collected on a Bruker AXS D8 VENTURE KAPPA diffractometer coupled to a PHOTON 100 CMOS detector with Mo Kα radiation (λ = 0.71073 Å) or with Cu Kα (λ = 1.54178 Å). For compound **8**, low-temperature (100 K) diffraction data (ϕ-and ω-scans) was collected on a Bruker AXS KAPPA APEX II diffractometer coupled to an APEX II CCD detector with graphite monochromated Mo Kα radiation (λ = 0.71073 Å). All diffractometer manipulations, including data collection, integration, and scaling were carried out using the Bruker APEXII software.[41] Absorption corrections were applied using SADABS.[42] Structures were solved by direct methods using SHELXS[43] and refined against F^2 on all data by full-matrix least squares with SHELXL-2016[44] using established

refinement techniques.[45] All non-hydrogen atoms were refined anisotropically. All hydrogen atoms were included into the model at geometrically calculated positions and refined using a riding model. The isotropic displacement parameters of all hydrogen atoms were fixed to 1.2 times the *U* value of the atoms they are linked to (1.5 times for methyl groups). All disordered atoms were refined with the help of similarity or distance restraints on the 1,2- and 1,3-distances and displacement parameters as well as enhanced rigid bond restraints for anisotropic displacement parameters. Due to the size of compounds most crystals included solvent accessible voids containing co-crystallized disordered solvent molecules. In most cases, this disorder could be modeled satisfactorily but the solution was not always ideal. These disordered solvent molecules were largely responsible for the alerts generated by the checkCIF protocol.

$LMn_3(OAc)(OTf)_2$

In the glovebox, to a yellow slurry of $LMn_3(OAc)_3$ (480.0 mg, 0.401 mmol) in CH_2Cl_2 (10 mL) was added dropwise methyl triflate (MeOTf; 0.132 mL, 1.203 mmol). During the course of ten minutes, the mixture became an opaque off-white suspension. After stirring for thirty minutes, all volatiles were removed under reduced pressure to yield an off-white powder. The solid was triturated in diethyl ether (10 mL), collected on a medium porosity glass frit, and washed with additional diethyl ether (3 × 10 mL). The solid was dried under vacuum to yield $LMn_3(OAc)(OTf)_2$ as an off-white powder. Yield 540 mg (98 %). ^{1}H NMR (300 MHz, CD_3CN): δ 63.9 (br), δ 43.7 (br), δ 11.01 (br), δ −10.8 (br). ^{19}F NMR (282 MHz, CD_2Cl_2): δ −76.9 (br). UV-Vis (CH_3CN) [ε (M^{-1} cm^{-1})]: 254 nm (6.4×10^4). Anal Calcd. for $C_{61}H_{42}F_6Mn_3N_6O_{11}S_2$: C 53.17, H 3.07, N 6.10. Found: C 52.93, H 3.28, N 6.36.

$[LMn_3(PhPz)_3OMn][OTf]_2$ (2)

In the glovebox, to thawing suspension of $LMn_3(OAc)(OTf)_2$ (550.0 mg, 0.401 mmol) in CH_2Cl_2 (5 mL) was added a thawing solution of NaPhPz (220.0 mg, 1.323 mmol) in THF (7 mL). The resulting suspension became homogeneous yellow-orange over the course of thirty minutes. After two hours, iodosobenzene (PhIO; 93.0 mg, 0.421 mmol) was added as a suspension in CH_2Cl_2 (2 mL), resulting in the formation of a purple slurry. After sixteen hours, the solvent was removed under reduced pressure, and the solids were triturated in diethyl ether (10 mL). The suspension was filtered over a Celite pad on top a coarse porosity glass frit, and subsequently washed with toluene (3 × 5 mL), and diethyl ether (10 mL). The remaining purple brown solid was collected using a minimal volume of CH_2Cl_2. Purple needles (500 mg) of the putative $[LMn_3(F_2ArPz)_3ONa]$ [OTf] (**1**) were obtained by vapor diffusion of diethyl either into a concentrated solution of **1** in CH_2Cl_2. The crystals were slurried in minimal THF (5 mL) and $Mn(OTf)_2(MeCN)_2$ (338.7 mg, 0.856 mmol) was added. During the course of one hour, the mixture turned brown-purple and was stirred for another sixteen hours. Next, the brown purple solids were collected on a Celite pad on top a coarse porosity glass, and washed with dimethoxyethane (DME; *ca.* 15 mL) until the purple filtrate became near-colorless. The remaining solid was collected with acetonitrile and dried under reduced pressure, yielding $[LMn_3(PhPz)_3OMn][OTf]_2$ as a brown-purple solid. Yield 512.0 mg (45 %). X-ray quality crystals of **2** were obtained by vapor diffusion of diethyl ether into a concentrated solution of 2 in acetonitrile. ^{1}H NMR (300 MHz, CD_2Cl_2): δ 50.0 (br), δ 35.2 (br), δ 31.2 (br), δ 13.3 (br), δ 10.61 (br), δ −12.4 (br), δ −19.0 (br). ^{19}F NMR

(282 MHz, CD_2Cl_2): δ −78.6 (s). UV-Vis (CH_2Cl_2) [ε (M^{-1} cm^{-1})]: 253 nm (8.9×10^4). Anal Calcd. for $C_{86}H_{60}F_6Mn_4N_{12}O_{10}S_2$: C 56.78, H 3.32, N 9.24. Found: C 56.37, H 3.37, N 9.54.

$[LMn_3(PhPz)_3OMn][OTf]_1$ (3)

In the glovebox, to a stirring solution of 2 (100.0 mg, 55.0 μmol) in CH_2Cl_2 (4 mL) was added cobaltocene ($CoCp_2$, 10.9 mg, 58.0 μmol). The color changed from brown-purple to red-purple, and after two hours the solvent was removed under reduced pressure. The solid was stirred as a purple suspension in DME (8 mL) and filtered over a Celite pad on top of a coarse porosity glass frit to remove cobaltocenium triflate. The remaining purple solid was eluted with CH_2Cl_2 (2 mL) and the solvent was removed under reduced pressure to yield $[LMn_3(PhPz)_3OMn][OTf]_1$ as a faint red purple solid. Yield 74.0 mg (81 %). X-ray quality crystals of **3** were obtained by vapor diffusion of diethyl ether into a solution of 3 in acetonitrile. ^{1}H NMR (300 MHz, CD_2Cl_2): δ 39.9 (br), δ 36.6 (br), δ 31.1 (br), δ 11.7 (br), δ −7.5 (br), δ −8.9 (br). ^{19}F NMR (282 MHz, CD_2Cl_2): − δ 78.8 (s). UV-Vis (CH_2Cl_2) [ε ($M^{δ1}$ $cm^{δ1}$)]: 256 nm (9.9×10^4), 371 nm (2.8×10^3). Anal Calcd. for C85H60F3Mn4N12O7S: C 61.12, H 3.62, N 10.06. Found: C 61.36, H 3.76, N 9.87.

$[LMn_3(PhPz)_2(OArPz)OMn][OTf]_2$ (5)

Procedure A—In the glovebox, to a stirring solution of **2** (320.0 mg, 0.18 mmol) in CH_2Cl_2 (10 mL) was added PhIO (40.3 mg, 0.18 mmol) as a suspension in CH_2Cl_2 (2 mL). During the course of one hour, the color changed to black, and the mixture turned homogeneous. The reaction was allowed to stir for sixteen hours, where after the solvent was removed under reduced pressure to yield an intense dark black/brown powder. The powder was triturated in toluene (*ca.* 6 mL), and the solid was collected on top of a coarse glass frit. The solid was washed with additional toluene *(ca.* 6 mL). and finally eluted with CH_2Cl_2 (4 mL). The solvent was removed under reduced pressure to yield $[LMn_3(PhPz)_2(OArPz)OMn][OTf]_2$ as a dark brown solid. Yield 310 mg (96 %). The ^{1}H NMR spectrum of 5 is identical to that from *Procedure B*.

Procedure B—In the glovebox, to a stirring solution of 6 (40.0 mg, 23.7 μmol) in CH_2Cl_2 (2 mL) was added silver triflate (AgOTf; 6.4 mg, 24.9 μmol) as a suspension in CH_2Cl_2 (2 mL). The solution darkened to off-black over the course of ten minutes. After two hours, the solution was filtered over a glass frit to remove metallic silver. The solvent was removed under reduced pressure to yield **5** as an off-black powder (39.8 mg, 90 %). ^{1}H NMR (300 MHz, CD_2Cl_2): δ 82.0 (br), δ 77.6 (br), δ 73.1 (br), δ 70.5 (br), δ 68.0 (br), δ 64.5 (br), δ 58.7 (br), δ 55.7 (br), δ 51.4 (br), δ 48.7 (br), δ 46.9 (br), δ 41.8 (br), δ 38.6 (br), δ 36.1 (br), δ 33.8 (br), δ 24.9 (br), δ 16.6 (br), δ 14.9 (br), δ 13.8 (br), δ 13.1 (br), δ 10.66 (br), δ –2.1 (br), δ – 3.5 (br), δ –4.5 (br), δ –10.1 (br), δ – 11.0 (br), δ –12.8 (br), δ – 14.4 (br), δ –17.2 (br), δ –19.4 (br), δ –20.7 (br), δ –21.9 (br), δ – 24.3 (br), δ –29.3 (br), δ –30.2 (br). ^{19}F NMR (282 MHz, CD_2Cl_2): – δ 78.8 (s). UV-Vis (CH_2Cl_2) [ε (M^{-1} cm^{-1})]: 245 nm (1.29×10^5), 371 nm (1.7×10^4). Anal Calcd. for $C_{86}H_{59}F_6Mn_4N_{12}O_{11}S_2 \cdot 2CH_2Cl_2$: C 53.16, H 3.24, N 8.45. Found: C 52.98, H 3.02, N 8.66.

[$LMn_3(PhPz)_2(OArPz)OMn$] [OTf] $_1$ (6)

Procedure A—In the glovebox, to a stirring solution of **3** (40.0 mg, 23.9 μmol) in CH_2Cl_2 (2 mL) was added PhIO (5.5 mg, 25.1 μmol) as a suspension in CH_2Cl_2 (2 mL). Over the course of one hour, the red-purple slurry became homogeneous and changed color to dark brown. After sixteen hours the solvent was removed under reduced pressure to yield a dark brown solid. The solid was triturated in benzene (3 mL) and filtered over a glass frit. The remaining solid was dissolved in CH_2Cl_2 (2 mL) and dried under reduced pressure to yield $[LMn_3(PhPz)_2(OArPz)OMn][OTf]_1$ as a dark brown solid. Yield 36.5 mg (92 %). The ^{1}H NMR spectrum of **6** was identical to that of Procedure B.

Procedure B—In the glovebox, to a solution of **2** (40.0 mg, 22.0 μmol) in CH_2Cl_2 (2 mL) was added NaOArPzH (4.4 mg, 24.2 μmol) in CH_2Cl_2 (2 mL). After thirty minutes, the reaction mixture darkened to black. After forty-eight hours, the solvent was removed under reduced pressure to give a brown black solid. The solid was triturated with benzene and collected on a glass frit. The remaining solid was washed with benzene (10 mL) and diethyl ether (5 mL), and finally eluted with CH_2Cl_2 (5 mL). The solvent was removed under reduced pressure to yield **6** as a brown/black solid. Yield 23.7 mg (85 %). ^{1}H NMR (300 MHz, CD_2Cl_2): δ 56.6 (br), δ 55.2 (br), δ 52.5 (br), δ 49.4 (br), δ 47.0 (br), δ 42.9 (br), δ 38.1 (br), δ 36.2 (br), δ 34.5 (br), δ 30.0 (br), δ 27.8 (br), δ 22.8 (br), δ 13.5 (br), δ 13.2 (br), δ 12.3 (br), δ 10.55 (br), δ −1.11 (br), δ −1.79 (br), δ −2.63 (br), δ −4.0 (br), δ −10.7 (br), δ −12.8 (br), δ −13.8 (br), δ −15.6 (br), δ −16.9 (br), δ −17.9 (br), δ −26.7 (br). ^{19}F NMR (282 MHz, CD2Cl2): − δ 78.8 (s). UV-Vis (CH_2Cl_2) [ε (M^{-1} cm^{-1})]: 251 nm (1.43×10^5), 355 nm (1.00×10^4), 513 nm (2.01×10^3). Anal Calcd. for $C_{85}H_{59}F_3Mn_4N_{12}O_8S$: C 60.58, H 3.53, N 9.97. Found: C 60.42, H 3.74, N 10.04.

[$LMn_3(F_2ArPz)_3OMn][OTf]_2$ (8)

In the glovebox, to a thawing suspension of $LMn_3(OAc)(OTf)_2$ (100.0 mg, 0.073 mmol) in CH_2Cl_2 (5 mL) was added a thawing solution of NaF_2ArPz (220.0 mg, 1.323 mmol) in THF (7 mL). During the course of thirty minutes, the resulting suspension became homogeneous and changed color to yellow-orange. After two hours, PhIO (16.8 mg, 0.076 mmol) was added as a suspension in CH_2Cl_2 (2 mL) resulting in the formation of a purple-brown slurry. After sixteen hours the solvent was removed under reduced pressure, and the solids were triturated with diethyl ether (15 mL). The suspension was filtered over a Celite pad on top a coarse porosity glass frit, and subsequently washed with benzene (20 mL), and diethyl ether (10 mL). The remaining purple-brown solid was collected using a minimal volume of CH_2Cl_2. Purple needles of the proposed $[LMn_3(F_2ArPz)_3ONa]$ [OTf] (**7**) were obtained by vapor diffusion of diethyl either into a concentrated solution of **7** in CH_2Cl_2. The crystals (50 mg) were slurried in minimal THF (5 mL) and $Mn(OTf)_2(MeCN)_2$ (60 mg, 0.057 mmol) was added. During the course of one hour, the mixture turned brown-violet and was stirred for another sixteen hours. The solvent was removed under reduced pressure to yield $[LMn_3(F_2ArPz)_3OMn]$ $[OTf]_2$ as a brown-violet solid. Yield 60 mg (45 %). X-ray quality crystals of **8** were obtained by vapor diffusion of diethyl ether into a concentrated solution of **8** in acetonitrile. ^{1}H NMR (300 MHz, CD_2Cl_2): δ 51.1 (br), δ 35.1 (br), δ 31.2 (br), δ 14.1 (br), δ 10.7 (br), S 8.4 (br), δ −11.9 (br), δ −19.6 (br). ^{19}F NMR (282 MHz, CD2Cl2): − δ 78.8 (s). UV-Vis (CH_2Cl_2) [ε (M^{-1} cm^{-1})]: 249 nm (9.9×10^4), 324 nm (4.5×10^3). Anal

Calcd. for $C_{86}H_{54}F_{12}Mn_4N_{12}O_{10}S_2$: C 53.60, H 2.82, N 8.72. Found: C 53.90, H 2.04, N 8.57.

[$LMn_3(F_2ArPz)_3OMn$] [OTf] (9)

In the glovebox, to a stirring solution of **8** (55.0 mg, 28 μmol) in THF (3 mL) was added $CoCp_2$ (5.7 mg, 30 μmol). The color changed from brown-violet to red-purple and after two hours the solvent was removed under reduced pressure. The solid was stirred as a violet suspension in DME (3 mL) and was subsequently filtered over a Celite pad on top a coarse porosity glass frit to remove cobaltocenium triflate. The remaining purple solid was collected in CH_2Cl_2 (2 mL) and dried under reduced pressure to yield [$LMn_3(F_2ArPz)_3OMn$] $[OTf]_1$ as a faint red-purple solid. Yield 30 mg (60 %). X-ray quality crystals of **9** were obtained by vapor diffusion of diethyl ether into a solution of **9** in CH_2Cl_2. ^{1}H NMR (300 MHz, CD_2Cl_2): δ 40.1 (br), δ 37.0 (br), δ 31.1 (br), δ 11.66 (br), δ 9.9 (br), δ −8.8 (br). ^{19}F NMR (282 MHz, CD2Cl2): − δ 78.8 (s). UV-Vis (CH2Cl2) [ε (M^{-1} cm^{-1})]: 249 nm (9.9×10^4), 324 nm (4.5×10^3). UV-Vis (CH_2Cl_2) [e (M^{-1} cm^{-1})]: 253 nm (7.6×10^4), 38 0 nm (2.9×10^3). Anal Calcd. for $C_{86}H_{54}F_9Mn_4N_{12}O_7S$: C 57.41, H 3.06, N 9.45. Found: C 57.66, H 3.43, N 8.89.

Addition of PhIO to [$LMn_3(F_2ArPz)_3OMn$][$OTf]_2$ (8)

In the glovebox, to a stirring solution of **8** (25.0 mg, 13.0 μmol) in CH_2Cl_2 (2 mL) was added PhIO (3.0 mg, 14.0 μmol) as a suspension in CH_2Cl_2 (1 mL). During the course of one hour, the color changed to black, and the mixture turned homogeneous. The reaction was allowed to stir for sixteen hours where after the solvent was removed under reduced pressure to yield a brown black powder. The powder was triturated in toluene (ca. 2 mL), collected on top a glass frit, and subsequently washed with additional toluene *(ca.* 2 mL). The remaining solid was dissolved in CH_2Cl_2, filtered, and the solvent was removed under reduced pressure to yield a brown-black powder. ESI-MS analysis is consistent with the formation of [$LMn_3(F_2PhPz)_2$(OFArPz)OMn][$OTf]_2$ (**10**) and [$LMn_3(F_2PhPz)_3$OMn(F)] $[OTf]_2$ (**11**).

Addition of PhIO to [$LMn_3(F_2ArPz)_3OMn$][$OTf]_1$ (9)

In the glovebox, to a stirring solution of **9** (20.0 mg, 11.0 μmol) in CH_2Cl_2 (2 mL) was added PhIO (2.5 mg, 11.0 μmol) as a suspension in CH_2Cl_2 (2 mL). During the course of one hour, the color changes to brown/black and the mixture turned homogeneous. The mixture was stirred for another sixteen hours, where after the solvent was removed under reduced pressure to yield a brown/black powder. The powder was triturated in toluene (ca. 2 mL), collected on top a glass frit, and subsequently washed with additional toluene *(ca.* 2 mL). The remaining solid was dissolved in CH_2Cl_2, filtered, and the solvent was removed under reduced pressure to yield a brown-black powder. ESI-MS analysis is consistent with the formation of [$LMn_3(F_2PhPz)_2$(OFArPz)OMn][$OTf]_1$ (**12**) and [LMn_3(F2PhPz)$_3$OMn(F)] $[OTf]_1$ (**13**).

Supplementary Material

Refer to Web version on PubMed Central for supplementary material.

Acknowledgments

This research was supported by the NIH (R01-GM102687B). T.A. is grateful for a Dreyfus fellowship. K.M.C. was a Larson Fellow and a recipient of the Caltech Summer Undergraduate Research Fellowship (SURF). We thank Michael K. Takase and Lawrence M. Henling for assistance in X-ray crystallography.

References

1. (a) Barber J. Mn_4Ca Cluster of Photosynthetic Oxygen-Evolving Center: Structure, Function and Evolution. Biochemistry. 2016; 55:5901–5906.(b) Yano J, Yachandra V. Mn_4Ca Cluster in Photosynthesis: Where and How Water is Oxidized to Dioxygen. Chem Rev. 2014; 114:4175–4205. [PubMed: 24684576] (c) Cox N, Pantazis DA, Neese F, Lubitz W. Biological Water Oxidation. Acc Chem Res. 2013; 46:1588–1596. [PubMed: 23506074] (d) Vinyard DJ, Ananyev GM, Dismukes GC. Photosystem II: The Reaction Center of Oxygenic Photosynthesis. Annu Rev Biochem. 2013; 82:577–606. [PubMed: 23527694]
2. (a) Young ID, Ibrahim M, Chatterjee R, Gul S, Fuller FD, Koroidov S, Brewster AS, Tran R, Alonso-Mori R, Kroll T, Michels-Clark T, Laksmono H, Sierra RG, Stan CA, Hussein R, Zhang M, Douthit L, Kubin M, de Lichtenberg C, Vo Pham L, Nilsson H, Cheah MH, Shevela D, Saracini C, Bean MA, Seuffert I, Sokaras D, Weng T-C, Pastor E, Weninger C, Fransson T, Lassalle L, Brauer P, Aller P, Docker PT, Andi B, Orville AM, Glownia JM, Nelson S, Sikorski M, Zhu D, Hunter MS, Lane TJ, Aquila A, Koglin JE, Robinson J, Liang M, Boutet S, Lyubimov AY, Uervirojnangkoorn M, Moriarty NW, Liebschner D, Afonine PV, Waterman DG, Evans G, Wernet P, Dobbek H, Weis WI, Brunger AT, Zwart PH, Adams PD, Zouni A, Messinger J, Bergmann U, Sauter NK, Kern J, Yachandra VK, Yan J. Structure of Photosystem II and Substrate Binding at Room Temperature. Nature. 2016; 540:453–457. [PubMed: 27871088] (b) Suga M, Akita F, Hirata K, Ueno G, Murakami H, Nakajima Y, Shimizu T, Yamashita K, Yamamoto M, Ago H, Shen JR. Native Structure of Photosystem II at 1.95 A Resolution Viewed by Femtosecond X-ray Pulses. Nature. 2015; 517:99–103. [PubMed: 25470056] (c) Umena Y, Kawakami K, Shen JR, Kamiya N. Crystal Structure of Oxygen-Evolving Photosystem II at a Resolution of 1.9 Å. Nature. 2011; 473:55–60. [PubMed: 21499260] (d) Ferreira KN, Iverson TM, Maghlaoui K, Barber J, Iwata S. Architecture of the Photosynthetic Oxygen Evolving Center. Science. 2004; 303:1831–1838. [PubMed: 14764885]
3. (a) Barber J. A Mechanism for Water Splitting and Oxygen Production in Photosynthesis. Nat Plants. 2017; 3:17041. [PubMed: 28368386] (b) Cox N, Retegan M, Neese F, Pantazis DA, Boussac A, Lubitz W. Electronic Structure Of the Oxygenevolving Complex in Photosystem II Prior to O-O Bond Formation. Science. 2014; 345:804–808. [PubMed: 25124437] (c) Navarro MP, Ames WM, Nilsson H, Lohmiller T, Pantazis DA, Rapatskiy L, Nowaczyk MM, Neese F, Boussac A, Messinger J. Ammonia Binding to the Oxygen Evolving Complex of Photosystem II Identifies the Solvent Exchangeable Oxygen Bridge (M-Oxo) of the Manganese Tetramer. Proc Natl Acad Sci. 2013; 110:15561–15566. [PubMed: 24023065] (d) Siegbahn PEM. Water Oxidation Mechanism in Photosystem II, Including Oxidations, Proton Release Pathways, O–O Bond Formation and O_2 Release. BBA-Bioenergetics. 2013; 1827:1003–1019. [PubMed: 23103385] (e) Limburg J, Szalai VA, Brudvig GW. A Mechanistic and Structural Model for the Formation and Reactivity Of A Mn^V=O Species in Photosynthetic Water Oxidation. J Chem Soc Dalton Trans. 1999:1353–1362.(f) Pecoraro VL, Baldwin MJ, Caudle MT, Hsieh WY, Law NA. A Proposal for Water Oxidation in Photosystem II. Pure Appl Chem. 1998; 70:925.
4. (a) Gray HB. Powering the Planet with Solar Fuel. Nat Chem. 2009; 1:1.(b) Lewis NS, Nocera DG. Powering the Planet: Chemical Challenges in Solar Energy Utilization. Proc Acad Natl Sci. 2006; 103:15729–15735.
5. (a) Paul S, Neese F, Pantazis DA. Structural Models of the Biological Oxygen-Evolving Complex: Achievements, Insights, and Challenges for Biomimicry. Green Chem. 2017(a) Gerey B, Gouré E, Fortage J, Pécaut J, Collomb MN. Manganese Calcium/Strontium Heterometallic Compounds and Their Relevance for the Oxygen-Evolving Center of Photosystem II. Coord Chem Rev. 2016; 319:1–24.(c) Blakemore JD, Crabtree RH, Brudvig GW. Molecular Catalysts for Water Oxidation. Chem Rev. 2015; 115:12974–13005. [PubMed: 26151088] (d) Tsui EY, Kanady JS, Agapie T. Synthetic Cluster Models of Biological and Heterogeneous Manganese Catalysts for O_2 Evolution. Inorg Chem. 2013; 52:13833–13848. [PubMed: 24328344] (e) Mullins CS, Pecoraro VL.

Reflections on Small Molecule Manganese Models that Seek to Mimic Photosynthetic Water Oxidation Chemistry. Coord Chem Rev. 2008; 252:416–443. [PubMed: 19081816] (f) Mukhopadhyay S, Mandal SK, Bhaduri S, Armstrong WH. Manganese Clusters with Relevance to Photosystem II. Chem Rev. 2004; 104:3981–4026. [PubMed: 15352784]

6. (a) Zhang C, Chen C, Dong H, Shen JR, Dau H, Zhao J. A Synthetic Mn_4Ca-Cluster Mimicking the Oxygen-Evolving Center of Photosynthesis. Science. 2015; 348:690. [PubMed: 25954008] (b) Kanady JS, Lin PH, Carsch KM, Nielsen RJ, Takase MK, Goddard WA, Agapie T. Toward Models for the Full Oxygen-Evolving Complex of Photosystem II by Ligand Coordination to Lower the Symmetry of the Mn_3CaO_4 Cubane: Demonstration that Electronic Effects Facilitate Binding of a Fifth Metal. J Am Chem Soc. 2014; 136:14373–14376. [PubMed: 25241826] (c) Mukherjee S, Stull JA, Yano J, Stamatatos TC, Pringouri K, Stich TA, Abboud KA, Britt RD, Yachandra VK, Christou G. Synthetic Model of the Asymmetric $[Mn_4CaO_4]$ Cubane Core of the Oxygen-Evolving Complex of Photosystem II. Proc Acad Natl Sci. 2012; 109:2257–2262.(d) Kanady JS, Tsui EY, Day MW, Agapie T. A Synthetic Model of the Mn_3Ca Subsite of the Oxygen-Evolving Complex in Photosystem II. Science. 2011; 333:733–736. [PubMed: 21817047]
7. (a) Song WJ, Seo MS, DeBeer George S, Ohta T, Song R, Kang M-J, Tosha T, Kitagawa T, Solomon EI, Nam W. Synthesis, Characterization, and Reactivities of Manganese(V)-Oxo Porphyrin Complexes. J Am Chem Soc. 2007; 129:1268–1277. [PubMed: 17263410] (b) Jin N, Ibrahim M, Spiro TG, Groves JT. Trans-dioxo Manganese(V) Porphyrins. J Am Chem Soc. 2007; 129:12416–12417. [PubMed: 17887684] (c) Shimazaki Y, Nagano T, Takesue H, Ye BH, Tani F, Naruta Y. Characterization of a Dinuclear Mn^{V}=O Complex and Its Efficient Evolution of O_2 in the Presence of Water. Angew Chem Int Ed. 2004; 43:98–100.(d) Jin N, Groves JT. Unusual Kinetic Stability of a Ground-State Singlet Oxomanganese(V) Porphyrin. Evidence for a Spin State Crossing Effect. J Am Chem Soc. 1999; 121:2923–2924.(e) Czernuszewicz RS, Su YO, Stern MK, Macor KA, Kim D, Groves JT, Spiro TG. Oxomanganese(IV) Porphyrins Identified by Resonance Raman and Infrared Spectroscopy. Weak Bonds and The Stability of the Half Filled t_{28} Subshell. J Am Chem Soc. 1988; 110:4158–4165.(f) Schappacher M, Weiss R. Formation of Manganese(IV)-Oxo Porphyrin Derivatives by Decomposition of Peroxycarbonate Complexes. Inorg Chem. 1987; 26:1189–1190.
8. (a) Kumar A, Goldberg I, Botoshansky M, Buchman Y, Gross Z. Oxygen Atom Transfer Reactions from Isolated (Oxo)manganese(V) Corroles to Sulfides. J Am Chem Soc. 2010; 132:15233–15245. [PubMed: 20932015] (b) Gao Y, Akermark T, Liu J, Sun L, Akermark B. Nucleophilic Attack of Hydroxide on a MnV Oxo Complex: A Model of the O–O Bond Formation in the Oxygen Evolving Complex of Photosystem II. J Am Chem Soc. 2009; 131:8726–8727. [PubMed: 19496534] (c) Gross Z, Golubkov G, Simkhovich L. Epoxidation Catalysis by a Manganese Corrole and Isolation of an Oxomanganese(V) Corrole. Angew Chem Int Ed. 2000; 39:4045–4047.
9. (a) Neu HM, Baglia RA, Goldberg DP. A Balancing Act: Stability versus Reactivity of Mn(o) Complexes. Acc Chem Res. 2015; 48:2754–2764. [PubMed: 26352344] (b) Mandimutsira BS, Ramdhanie B, Todd RC, Wang H, Zareba AA, Czernuszewicz RS, Goldberg DP. A Stable Manganese(V)-Oxo Corrolazine Complex. J Am Chem Soc. 2002; 124:15170–15171. [PubMed: 12487581]
10. (a) Hong S, Lee YM, Sankaralingam M, Vardhaman AK, Park YJ, Cho KB, Ogura T, Sarangi R, Fukuzumi S, Nam W. A Manganese(V)-Oxo Complex: Synthesis by Dioxygen Activation and Enhancement of Its Oxidizing Power by Binding Scandium Ion. J Am Chem Soc. 2016; 138:8523–8532. [PubMed: 27310336] (b) Barman P, Vardhaman AK, Martin B, Worner SJ, Sastri CV, Comba P. Influence of Ligand Architecture on Oxidation Reactions by High-Valent Nonheme Manganese Oxo Complexes Using Water as a Source of Oxygen. Angew Chem Int Ed. 2015; 54:2095–2099.(c) Yin G. Understanding the Oxidative Relationships of the Metal Oxo, Hydroxo, and Hydroperoxide Intermediates with Manganese(IV) Complexes Having Bridged Cyclams: Correlation of the Physicochemical Properties with Reactivity. Acc Chem Res. 2013; 46:483–492. [PubMed: 23194251] (d) Kurahashi T, Kikuchi A, Tosha T, Shiro Y, Kitagawa T, Fujii H. Transient Intermediates from Mn(salen) with Sterically Hindered Mesityl Groups: Interconversion between Mn^{IV}-Phenolate and Mn^{III} Phenoxyl Radicals as an Origin for Unique Reactivity. Inorg Chem. 2008; 47:1674–1686. [PubMed: 18237118] (e) Popescu DL, Chanda A, Stadler M, de Oliveira FT, Ryabov AD, Münck E, Bominaar EL, Collins TJ. High-Valent First-Row Transition-Metal Complexes of Tetraamido (4N) and Diamidodialkoxido or Diamidophenolato (2N/2O)

Ligands: Synthesis, Structure, and Magnetochemistry. Coord Chem Rev. 2008; 252:2050–2071.(f) Yin G, McCormick JM, Buchalova M, Danby AM, Rodgers K, Day VW, Smith K, Perkins CM, Kitko D, Carter JD, Scheper WM, Busch DH. Synthesis, Characterization, and Solution Properties of a Novel Cross-Bridged Cyclam Manganese(IV) Complex Having Two Terminal Hydroxo Ligands. Inorg Chem. 2006; 45:8052–8061. [PubMed: 16999402] (g) MacDonnell FM, Fackler NLP, Stern C, O'Halloran TV. Air Oxidation of a Five-Coordinate Mn(III) Dimer to a High-Valent Oxomanganese(V) Complex. J Am Chem Soc. 1994; 116:7431–7432.(h) Collins TJ, Powell RD, Slebodnick C, Uffelman ES. A Water-Stable Manganese(V)-Oxo Complex: Definitive Assignment of a $v_{Mn\equiv O}$ Infrared Vibration. J Am Chem Soc. 1990; 112:899–901.

11. Shirin Z, Hammes BS, Young VG, Borovik AS. Hydrogen Bonding in Metal Oxo Complexes: Synthesis and Structure of a Monomeric Manganese(III)-Oxo Complex and its Hydroxo Analogue. J Am Chem Soc. 2000; 122:1836–1837.
12. Parsell TH, Behan RK, Green MT, Hendrich MP, Borovik AS. Preparation and Properties of a Monomeric Mn^{IV}–Oxo Complex. J Am Chem Soc. 2006; 128:8728–8729. [PubMed: 16819856]
13. Taguchi T, Gupta R, Lassalle-Kaiser B, Boyce DW, Yachandra VK, Tolman WB, Yano J, Hendrich MP, Borovik AS. Preparation and Properties of a Monomeric HighSpin Mn^{V}-Oxo Complex. J Am Chem Soc. 2012; 134:1996–1999. [PubMed: 22233169]
14. Gupta R, Taguchi T, Lassalle-Kaiser B, Bominaar EL, Yano J, Hendrich MP, Borovik AS. High-Spin Mn–Oxo Complexes and Their Relevance to the Oxygen-Evolving Complex within Photosystem II. Proc Natl Acad Sci. 2015; 112:5319–5324. [PubMed: 25852147]
15. Britt RD, Suess DLM, Stich TA. An Mn(V)-Oxo Role in Splitting Water? Proc Natl Acad Sci. 2015; 112:5265–5266. [PubMed: 25883270]
16. Park YJ, Matson EM, Nilges MJ, Fout AR. Exploring Mn O Bonding in the Context of an Electronically Flexible Secondary Coordination Sphere: Synthesis of a Mn(III)-Oxo. Chem Commun. 2015; 51:5310–5313.
17. Limburg J, Vrettos JS, Liable-Sands LM, Rheingold AL, Crabtree RH, Brudvig GW. A Functional Model for O-O Bond Formation by the O_2-Evolving complex in Photosystem II. Science. 1999; 283:1524–1527. [PubMed: 10066173]
18. (a) Vaddypally S, Kondaveeti SK, Karki S, Van Vliet MM, Levis RJ, Zdilla MJ. Reactive Pendant Mn=O in a Synthetic Structural Model of a Proposed S_4 State in the Photosynthetic Oxygen Evolving Complex. J Am Chem Soc. 2017; 139:4675–4681. [PubMed: 28288514] (b) de Ruiter G, Carsch KM, Gul S, Chatterjee R, Thompson NB, Takase MK, Yano J, Agapie T. Accelerated Oxygen Atom Transfer and C-H Bond Oxygenation by Remote Redox Changes in Fe3Mn-Iodosobenzene Adducts. Angew Chem Int Ed. 2017; 56:4772–4776.
19. Khenkin AM, Kumar D, Shaik S, Neumann R. Characterization of Manganese(V)-Oxo Polyoxometalate Intermediates and Their Properties in Oxygen-Transfer Reactions. J Am Chem Soc. 2006; 128:15451–15460. [PubMed: 17132012]
20. (a) de Ruiter G, Thompson NB, Takase MK, Agapie T. Intramolecular C-H and C-F Bond Oxygenation Mediated by a Putative Terminal Oxo Species in Tetranuclear Iron Complexes. J Am Chem Soc. 2016; 138:1486–1489. [PubMed: 26760217] (b) Han Z, Horak KT, Lee HB, Agapie T. Tetranuclear Manganese Models of the OEC Displaying Hydrogen Bonding Interactions: Application to Electrocatalytic Water Oxidation to Hydrogen Peroxide. J Am Chem Soc. 2017 just accepted.
21. Reports of oxygenation of $C(sp^2)$-H bonds by mononuclear complexes include:(a) Aratani Y, Yamada Y, Fukuzumi S. Selective Hydroxylation of Benzene Derivatives and Alkanes with Hydrogen Peroxide Catalysed by a Manganese Complex Incorporated Into Mesoporous Silica-Alumina. Chem Commun. 2015; 51:4662–4665.(b) Wu X, Seo MS, Davis KM, Lee YM, Chen J, Cho KB, Pushkar YN, Nam W. A Highly Reactive Mononuclear Non-Heme Manganese(IV)-Oxo Complex that can Activate the Strong C–H Bonds of Alkanes. J Am Chem Soc. 2011; 133:20088–20091. [PubMed: 22091637] (c) Sawant SC, Wu X, Cho J, Cho KB, Kim SH, Seo MS, Lee YM, Kubo M, Ogura T, Shaik S, Nam W. Water as an Oxygen Source: Synthesis, Characterization, and Reactivity Studies of a Mononuclear Nonheme Manganese(IV) Oxo Complex. Angew Chem Int Ed. 2010; 49:8190–8194.

22. de Ruiter G, Thompson NB, Lionetti D, Agapie T. Nitric Oxide Activation by Distal Redox Modulation in Tetranuclear Iron Nitrosyl Complexes. J Am Chem Soc. 2015; 137:14094–14106. [PubMed: 26390375]

23. (a) Kanady JS, Tran R, Stull JA, Lu L, Stich TA, Day MW, Yano J, Britt RD, Agapie T. Role of Oxido Incorporation and Ligand Lability in Expanding Redox Accessibility of Structurally Related Mn_4 Clusters. Chem Sci. 2013; 4:3986–3996. [PubMed: 24163730] (b) Yang CI, Wernsdorfer W, Tsai YJ, Chung G, Kuo TS, Lee GH, Shieh M, Tsai HL. Mixed-Valence Tetra and Hexanuclear Manganese Complexes from the Flexibility of Pyridine-Containing β-Diketone Ligands. Inorg Chem. 2008; 47:1925–1939. [PubMed: 18290611] (c) Zaleski CM, Weng TC, Dendrinou-Samara C, Alexiou M, Kanakaraki P, Hsieh WY, Kampf J, Penner-Hahn JE, Pecoraro VL, Kessissoglou DP. Structural and Physical Characterization of Tetranuclear [$Mn^{II}_3Mn^{IV}$] and [$Mn^{II}_2Mn^{III}_2$] Valence-Isomer Manganese Complexes. Inorg Chem. 2008; 47:6127–6136. [PubMed: 18537236] (d) Cotton FA, Daniels LM, Jordan GT Iv, Murillo* CA, Pascual I. Structural Variations in the Ligands Around a Simple Oxo-Centered Building Block, the Tetrahedral $[M4O]^{6+}$ Unit, M = Mn and Fe. Inorg Chim Acta. 2000; 297:6–10.(e) McKee V, Tandon SS. X-Ray Crystal Structure and Some Properties of a Tetranuclear, Mixed-Valence Manganese Complex of a Macrocyclic Ligand. J Chem Soc Chem Commun. 1988:1334–1336.

24. Addison AW, Rao TN, Reedijk J, van Rijn J, Verschoor GC. Synthesis, Structure, and Spectroscopic Properties of Copper(Ii) Compounds Containing Nitrogen-Sulphur Donor Ligands; The Crystal and Molecular Structure of Aqua[1,7-Bis(N methylbenzimidazol-2′-yl)-2,6-Dithiaheptane]Copper(II) Perchlorate. J Chem Soc Dalton Trans. 1984:1349–1356.

25. (a) Guillet GL, Sloane FT, Ermert DM, Calkins MW, Peprah MK, Knowles ES, Cizmar E, Abboud KA, Meisel MW, Murray LJ. Preorganized Assembly of Three Iron(II) or Manganese(II) *β*-Diketiminate Complexes Using a Cyclophane Ligand. Chem Commun. 2013; 49:6635–6637.(b) Fout AR, Xiao DJ, Zhao Q, Harris TD, King ER, Eames EV, Zheng SL, Betley TA. Trigonal Mn and Co_3 Clusters Supported by Weak-Field Ligands: A Structural, Spectroscopic, Magnetic, and Computational Investigation into the Correlation of Molecular and Electronic Structure. Inorg Chem. 2012; 51:10290–10299. [PubMed: 22991939]

26. Betley TA, Wu Q, Van Voorhis T, Nocera DG. Electronic Design Criteria for O–O Bond Formation via Metal-Oxo Complexes. Inorg Chem. 2008; 47:1849–1861. [PubMed: 18330975]

27. (a) McGarrigle EM, Gilheany DG. Chromium and Manganese-salen Promoted Epoxidation of Alkenes. Chem Rev. 2005; 105:1563–1602. [PubMed: 15884784] (b) Linker T. The Jacobsen-Katsuki Epoxidation and its Controversial Mechanism. Angew Chem Int Ed. 1997; 36:2060–2062. (c) Brandes BD, Jacobsen EN. Highly Enantioselective, Catalytic Epoxidation of Trisubstituted Olefins. J Org Chem. 1994; 59:4378–4380.(d) Groves JT, Stern MK. Olefin Epoxidation by Manganese(IV) Porphyrins: Evidence for Two Reaction Pathways. J Am Chem Soc. 1987; 109:3812–3814.

28. Song WJ, Seo MS, George SD, Ohta T, Song R, Kang MJ, Tosha T, Kitagawa T, Solomon EI, Nam W. Synthesis, Characterization, and Reactivities of Manganese(V)-Oxo Porphyrin Complexes. J Am Chem Soc. 2007; 129:1268–1277. [PubMed: 17263410]

29. Lee JY, Lee YM, Kotani H, Nam W, Fukuzumi S. HighValent Manganese(V)–Oxo Porphyrin Complexes in Hydride Transfer Reactions. Chem Commun. 2009:704–706.

30. Liu SY, Soper JD, Yang JY, Rybak-Akimova EV, Nocera DG. Mechanistic Studies of Hangman Salophen-Mediated Activation of O–O Bonds. Inorg Chem. 2006; 45:7572–7574. [PubMed: 16961343]

31. (a) Garcia-Bosch I, Cowley RE, Diaz DE, Peterson RL, Solomon EI, Karlin KD. Substrate and Lewis Acid Coordination Promote O–O Bond Cleavage of an Unreactive $L^2Cu^{II}_2(O_2^{2-})$ Species to form $L_2Cu^{III}_2(O)_2$ Cores with Enhanced Oxidative Reactivity. J Am Chem Soc. 2017; 139:3186–3195. [PubMed: 28195739] (b) Sahu S, Zhang B, Pollock CJ, Dürr M, Davies CG, Confer AM, Ivanović Burmazovic I, Siegler MA, Jameson GNL, Krebs C, Goldberg DP. Aromatic C-F Hydroxylation by Nonheme Iron(IV)-Oxo Complexes: Structural, Spectroscopic, and Mechanistic Investigations. J Am Chem Soc. 2016; 138:1279112802.(c) Colomban C, Kudrik EV, Afanasiev P, Sorokin AB. Catalytic Defluorination of Perfluorinated Aromatics under Oxidative Conditions Using N-Bridged Diiron Phthalocyanine. J Am Chem Soc. 2014; 136:11321–11330. [PubMed: 25031156] (d) Sahu S, Quesne MG, Davies CG, Dürr M, Ivanovic-Burmazovic I, Siegler MA, Jameson GNL, de Visser SP, Goldberg DP. Direct Observation of a Nonheme

Iron(IV)–Oxo Complex that Mediates Aromatic C-F Hydroxylation. J Am Chem Soc. 2014; 136:13542–13545. [PubMed: 25246108] (e) Serrano-Plana J, Garcia-Bosch I, Miyake R, Costas M, Company A. Selective Ortho-Hydroxylation-Defluorination of 2-Fluorophenolates with a Bis(μ-oxo)dicopper(III) Species. Angew Chem Int Ed. 2014; 53:9608–9612.(f) Ohe T, Mashino T, Hirobe M. Novel Oxidative Pathway of Para-Substituted Phenols in Cytochrome P450 Chemical Model: Substituent Elimination Accompanying Ipso-Substitution by the Oxygen Atom of the Active Species. Tetrahedron Lett. 1995; 36:7681–7684.For examples of C–F bond hydroxylation with P450 enzymes, see:(g) Ohe T, Mashino T, Hirobe M. Substituent Elimination From p-Substituted Phenols by Cytochrome P450. Drug Metab Dispos. 1997; 25:116–122. [PubMed: 9010638] (h) Cnubben NHP, Vervoort J, Boersma MG, Rietjens IMCM. The Effect of Varying Halogen Substituent Patterns on the Cytochrome P450 Catalysed Dehalogenation of 4-Halogenated Anilines to 4-Aminophenol Metabolites. Biochem Pharmacol. 1995; 49:1235–1248. [PubMed: 7763304] (i) den Besten C, van Bladeren PJ, Duizer E, Vervoort J, Rietjens IMCM. Cytochrome P450-Mediated Oxidation of Pentafluorophenol to Tetrafluorobenzoquinone as the Primary Reaction Product. Chem Res Toxicol. 1993; 6:674–680. [PubMed: 8292746] (j) Cnubben NHP, Vervoort J, Veeger C, Rietjens IMCM. Study on the Regioselectivity and Mechanism of the Aromatic Hydroxylation of Monofluoroanilines. Chem-Biol Interact. 1992; 85:151–172. [PubMed: 1493607] (k) Rietjens IMCM, Vervoort JA. New Hypothesis for the Mechanism for Cytochrome P-450 Dependent Aerobic Conversion of Hexahalogenated Benzenes to Pentahalogenated Phenols. Chem Res Toxicol. 1992; 5:10–19. [PubMed: 1581524] (l) Rietjens IMCM, Vervoort J. Bioactivation of 4-Fluorinated Anilines to Benzoquinoneimines as Primary Reaction Products. Chem-Biol Interact. 1991; 77:263–281. [PubMed: 2009574] (m) Rietjens IMCM, Tyrakowska B, Veeger C, Vervoort J. Reaction Pathways for Biodehalogenation of Fluorinated Anilines. Eur J Biochem. 1990; 194:945–954. [PubMed: 2269311] (n) Rietjens IMCM, Vervoort J. Microsomal Metabolism of Fluoroanilines. Xenobiotica. 1989; 19:1297–1305. [PubMed: 2618082]

32. Haynes, WM., editor. CRC Handbook of Chemistry and Physics. 93rd. CRC Press; 2013. p. 2668
33. We recently submitted a manuscript describing the first example of C-F bond activation mediated by a putative terminal manganese-oxo species cluster attached to a cluster. The focus of this manuscript is the selectivity of CH vs CF bond activation with Fe and Mn clusters. It will be referenced as follows:de Ruiter G, Carsch KM, Takase MK, Agapie T. Journal. 2017 etc.
34. (a) Leeladee P, Goldberg DP. Epoxidations Catalyzed by Manganese(V) Oxo and Imido Complexes: Role of the Oxidant Mn-Oxo (Imido) Intermediate. Inorg Chem. 2010; 49:3083–3085. [PubMed: 20201529] (b) Birchall T, Smegal JA, Hill CL. Iodine-127 Mossbauer Study of Some Phenyl-Iodine Compounds and the Alkane Activating Manganese Porphyrin Complexes Containing Iodosylbenzene Ligands. Inorg Chem. 1984; 23:1910–1913.(c) Smegal JA, Schardt BC, Hill CL. Isolation, Purification, and Characterization of Intermediate (Iodosylbenzene) Metalloporphyrin Complexes from the (Tetraphenylporphinato) Manganese(III) Iodosylbenzene Catalytic Hydrocarbon Functionalization System. J Am Chem Soc. 1983; 105:3510–3515.
35. (a) Shaik S, Milko P, Schyman P, Usharani D, Chen H. Trends in Aromatic Oxidation Reactions Catalyzed by Cytochrome P450 Enzymes: A Valence Bond Modeling. J Chem Theory Comput. 2011; 7:327–339. [PubMed: 26596155] (b) Shaik S, Cohen S, Wang Y, Chen H, Kumar D, Thiel W. P450 Enzymes: Their Structure, Reactivity, and Selectivity-Modeled by QM/MM Calculations. Chem Rev. 2010; 110:949–1017. [PubMed: 19813749] (c) Shaik S, Kumar D, de Visser SP, Altun A, Thiel W. Theoretical Perspective on the Structure and Mechanism of Cytochrome P450 Enzymes. Chem Rev. 2005; 105:2279–2328. [PubMed: 15941215] (d) Bathelt CM, Ridder L, Mulholland AJ, Harvey JN. Aromatic Hydroxylation by Cytochrome P450: Model Calculations of Mechanism and Substituent Effects. J Am Chem Soc. 2003; 125:15004–15005. [PubMed: 14653732]
36. (a) Bigi JP, Harman WH, Lassalle-Kaiser B, Robles DM, Stich TA, Yano J, Britt RD, Chang CJ. A High-Spin Iron(IV)-Oxo Complex Supported by a Trigonal Nonheme Pyrrolide Platform. J Am Chem Soc. 2012; 134:1536–1542. [PubMed: 22214221] (b) Harman WH, Chang CJ. N_2O Activation and Oxidation Reactivity from a Non-Heme Iron Pyrrole Platform. J Am Chem Soc. 2007; 129:15128–15129. [PubMed: 18004860]
37. Hackett JC, Sanan TT, Hadad CM. Oxidative Dehalogenation of Perhalogenated Benzenes by Cytochrome P450 Compound I. Biochemistry. 2007; 46:5924–5940. [PubMed: 17455915]

38. Saltzman, H., Sharefkin, JG. Org Synth. John Wiley & Sons, Inc; 2003. Iodosobenzene.
39. Bochmann M, Jaggar AJ, Wilson LM, Hursthouse MB, Motevalli M. Synthesis of Cationic Alkyl Bis(cyclopentadienyl)Titanium Complexes by One-Electron Oxidation of Titanium(III) Alkyls. The Structure Of $[Cp_2*TiMe(TTH)]BPh_4$ and $[Cp_2*Ti(OH)(H_2O)]BPh_4$•2THF. Polyhedron. 1989; 8:1838–1843.
40. Riedel PJ, Arulsamy N, Mehn MP. Facile Routes to Manganese(II) Triflate Complexes. Inorg Chem Commun. 2011; 14:734–737. [PubMed: 21660114]
41. APEX-II. Version 2 User Manual, M86-E01078, Bruker Analytical X-ray Systems. Madison, WI: Jun. 2006
42. Sheldrick, GM. SADABS (version 2008/1): Program for Absorption Correction for Data from Area Detector Frames. University of Göttingen; 2008.
43. Sheldrick G. Phase annealing in SHELX-90: Direct Methods for Larger Structures. Acta Crystallogr, Sect A. 1990; 46:467–473.
44. Sheldrick GM. A Short History of SHELX. Acta Crystallogr, Sect A: Found Crystallogr. 2008; 64:112–122.
45. Müller P. Practical Suggestions for Better Crystal Structures. Crystallogr Rev. 2009; 15:57–83.

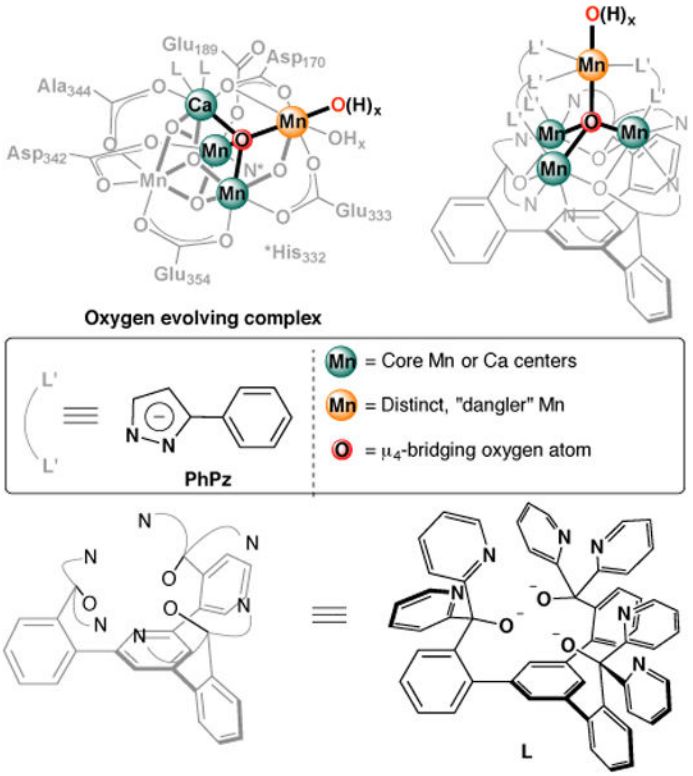

Figure 1.

Structural similarity of tetranuclear manganese clusters $[LMn_3(PhPz)\ 3OMn(O)]^{n+}$ (n = 1 or 2; top right) reported here to the oxygen evolving complex (OEC) in photosystem II (top left). The metal centers are supported by pyrazolates (inset) and a 1,3,5-triarylbenzene-based ligand (L).

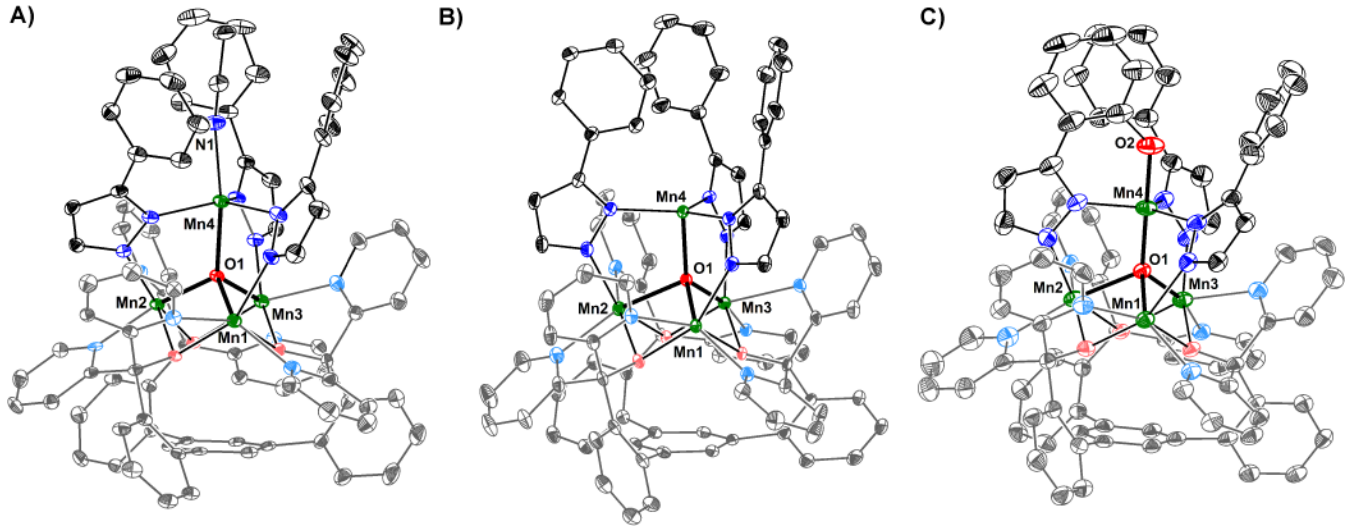

Figure 2.

Solid-state structure of (A) $[LMn_3(PhPz)_3OMn][OTf]_2$ (**2**), (B) $[LMn_3(PhPz)_3OMn][OTf]_1$ (**3**), and (C) $[LMn_3(PhPz)_2(OArPz)OMn][BPh_4]_1$ (**6′**). Thermal ellipsoids are shown at the 50% probability level. Hydrogen atoms, outer sphere counter ions, and co-crystallized solvent molecules are omitted for clarity. See Table 1 for selected bond angles and distances.

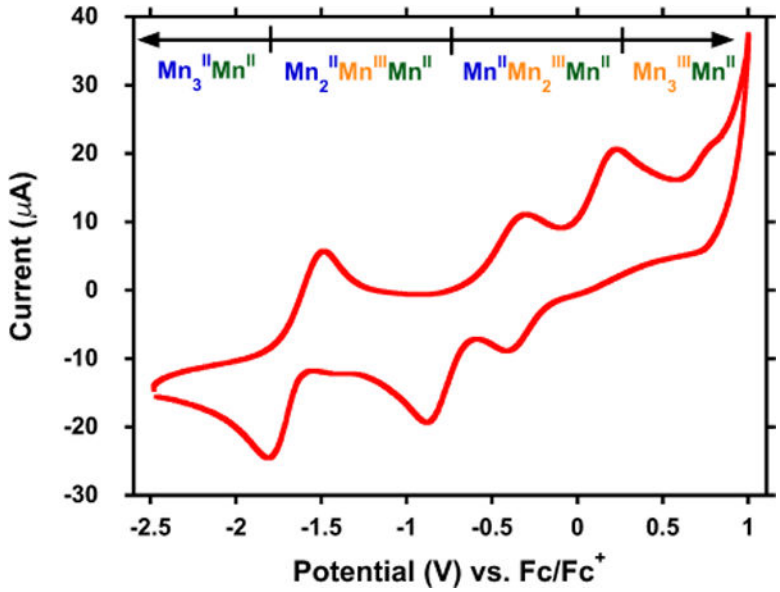

Figure 3.

Cyclic voltammogram of $[LMn_3(PhPz)_3OMn]\,[OTf]_2$ **(2)** recorded at 100 mV s^{-1} in dichloromethane at a 2 mM concentration. The recorded potentials are referenced against the Fc/Fc^+ redox couple.

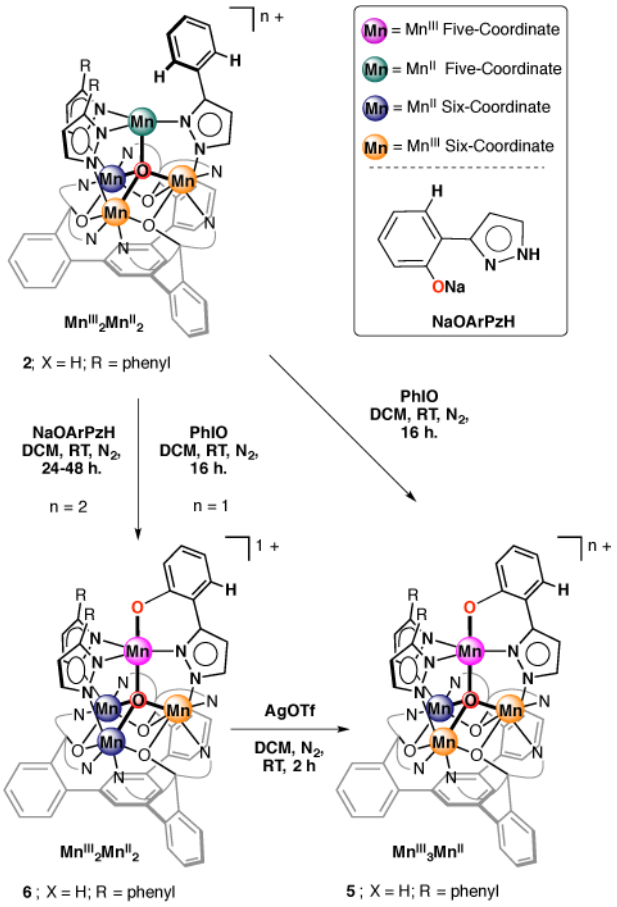

Figure 4.
Reactivity of complex **2** with PhIO, and independent syntheses of complexes **5** and **6**.

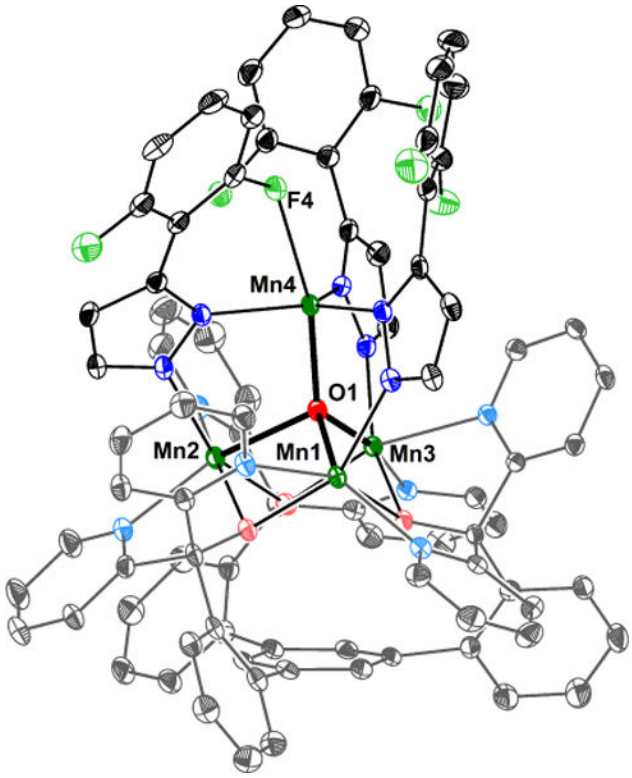

Figure 5.

Solid-state structure of $[LMn_3(F_2ArPz)_3OMn]\ [OTf]_1$ (**9**), showing a weak interaction between Mn4 and the *ortho* fluorine (F4) of the pyrazolate ligand. Thermal ellipsoids are shown at the 50% probability level. Hydrogen atoms, outer sphere counter ions, and co-crystallized solvent molecules are omitted for clarity

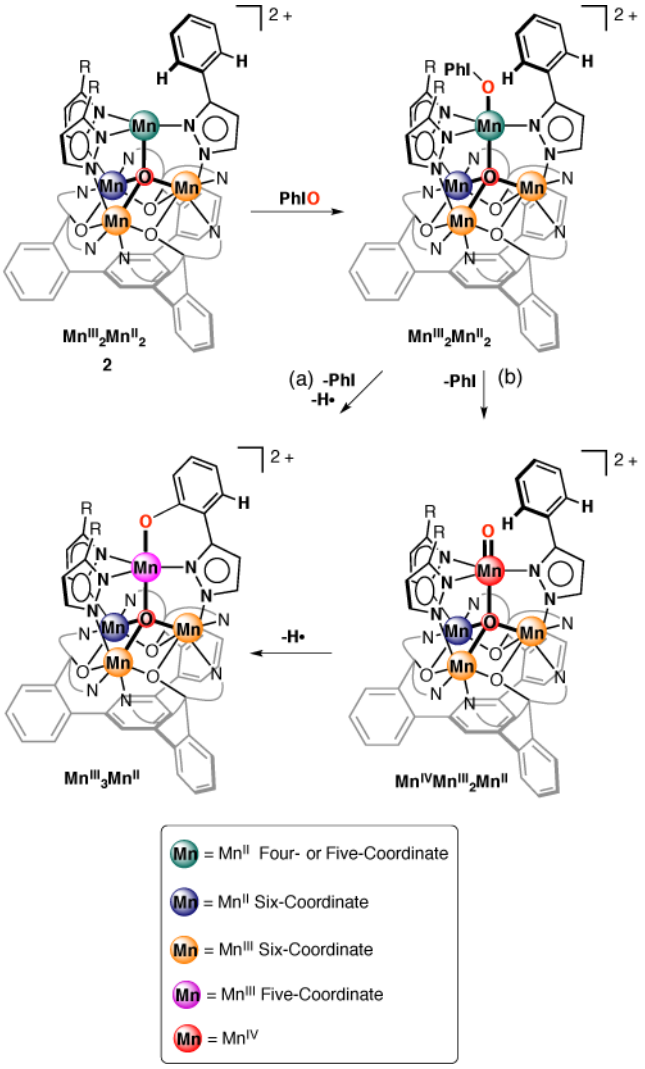

Figure 6.

Proposed mechanisms for arene hydroxylation observed with complex 2 via: (a) direct C–H insertion by an iodosobenzene adduct, (b) a high-valent Mn-oxo. Both paths require the loss of a hydrogen atom to access the final observed product.

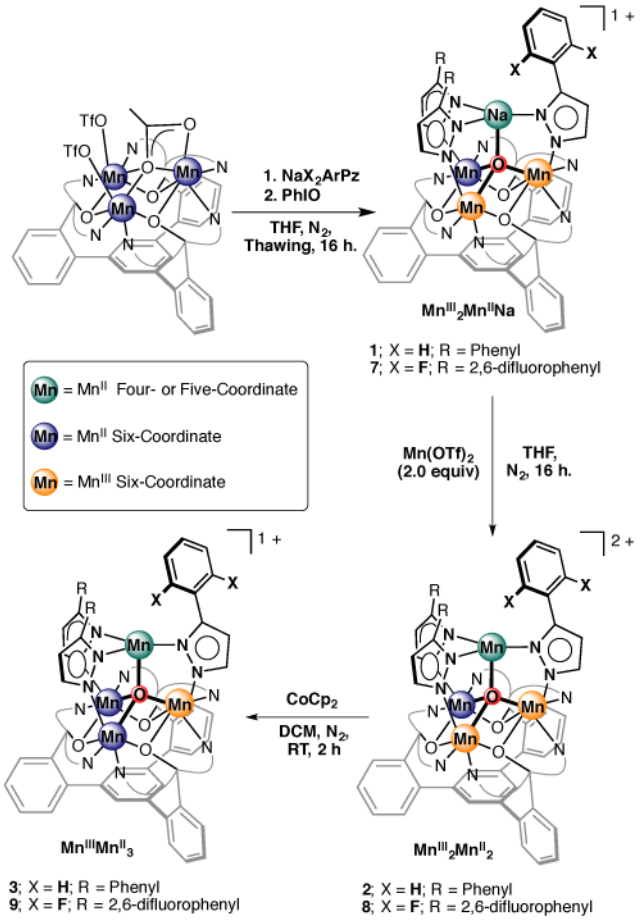

Scheme 1.
Synthesis of complexes **1–3** and **7–9**.

Table 1

Select bond distances and angles for Complexes **2**, **3**, **6′**, **8**, and **9**.

Bond Distances (Å)	Complex				
	2	**3**	**6′**	**8**	**9**
Mn1–O1	2.240(3)	2.116(2)	2.179(3)	2.216(3)	2.127(1)
Mn2–O1	1.886(3)	2.189(2)	2.247(3)	1.914(3)	2.192(2)
Mn3–O1	1.891(3)	1.816(1)	1.094(3)	1.892(3)	1.801(1)
Mn4–O1	2.108(3)	1.987(1)	1.851(3)	2.098(3)	2.012(1)
Mn4–O2	–	–	1.842(4)	–	–
Mn1–N11	2.202(3)	2.210(2)	2.201(4)	2.331(5)	2.234(2)
Mn1–N12	2.361(3)	2.346(2)	2.382(4)	2.171(4)	2.349(2)
Mn1–N13	2.159(4)	2.255(2)	2.220(4)	2.164(2)	2.247(2)
Mn2–N21	2.076(4)	2.234(2)	2.214(4)	2.216(4)	2.220(2)
Mn2–N22	2.318(3)	2.373(2)	2.341(4)	2.103(5)	2.239(2)
Mn2–N23	2.011(3)	2.197(2)	2.154(4)	2.007(5)	2.189(2)
Mn3–N31	2.108(3)	2.072(2)	2.092(4)	2.304(4)	2.072(2)
Mn3–N32	2.195(3)	2.377(2)	2.338(4)	2.089(4)	2.332(2)
Mn3–N33	1.998(3)	2.099(2)	2.033(4)	2.024(5)	2.097(2)
Mn4–N14	2.194(4)	2.122(2)	2.042(4)	2.138(4)	2.143(2)
Mn4–N24	2.170(3)	2.109(2)	2.013(4)	2.194(5)	2.134(2)
Mn4–N34	2.202(3)	2.131(2)	2.106(4)	2.187(5)	2.149(2)
N13–N14	1.381(6)	1.379(3)	1.380(6)	1.383(6)	1.369(3)
N23–N24	1.382(5)	1.380(2)	1.369(6)	1.375(7)	1.372(3)
N33–N34	1.384(6)	1.379(2)	1.375(6)	1.378(6)	1.376(3)
Bond Angles (°)					
N14–Mn4–N24	111.9(1)	118.19(7)	129.8(2)	116.0(2)	111.86(7)
N24–Mn4–N34	124.9(1)	120.44(7)	109.8(2)	126.5(2)	123.37(7)
N34–Mn4–N14	119.9(1)	120.63(7)	120.3(2)	114.8(2)	124.72(7)
Torsion Angles (°)					

Bond Distances (Å)	Complex				
	2	**3**	**6′**	**8**	**9**
Mn1–N13–N14–Mn4	30.4(4)	3.5(2)	26.9(4)	−10.5(5)	1.7(2)
Mn2–N23–N24–Mn4	31.2(3)	−5.1(2)	−5.5(5)	−3.6(5)	20.8(2)
Mn3–N33–N34–Mn4	5.3(4)	2.7(2)	21.4(4)	−22.6(5)	−0.6(2)
Centroid Distances (Å)					
Mn1|Mn2|Mn3–N14|N24|N34	2.772	2.925	2.860	2.801	2.945
Mn1|Mn2|Mn3–O11|O21|O31	1.150	1.127	1.096	1.162	1.111
N14|N24|N34–O11|O21|O31	3.921	4.046	3.948	3.959	4.055
Mn1|Mn2|Mn3–O1	0.913	0.962	1.049	0.924	0.958